Proceedings of the ASME 2021 40th International Conference on Ocean, Offshore and Arctic Engineering
OMAE2021
June 21-30, 2021, Virtual, Online

OMAE2021-62181

DRAFT: ESTIMATION OF WIND TURBINE GEARBOX LOADS FOR ONLINE FATIGUE MONITORING USING INVERSE METHODS

Felix C. Mehlan*, Amir R. Nejad, Zhen Gao
Department of Marine Technology (IMT)
Norwegian University of Science and Technology (NTNU)
Trondheim, 7491
Norway
felix.c.mehlan@ntnu.no

ABSTRACT

In this article a novel approach for the estimation of wind turbine gearbox loads with the purpose of online fatigue damage monitoring is presented. The proposed method employs a Digital Twin framework and aims at continuous estimation of the dynamic states based on CMS vibration data and generator torque measurements from SCADA data. With knowledge of the dynamic states local loads at gearbox bearings are easily determined and fatigue models are be applied to track the accumulation of fatigue damage. A case study using a simulation measurements from a high-fidelity gearbox model is conducted to evaluate the proposed method. The estimated loads at the considered IMS and HSS bearings show moderate to high correlation ($R = 0.50 - 0.96$) to the measurements, as lower frequency internal dynamics are not fully captured. The estimated fatigue damage differs by $5 - 15$ *% from measurements.*

INTRODUCTION

Recent trends show an increased shift towards offshore wind turbine installations due to the higher energy yield and fewer issues with land displacement and noise [1]. However, offshore sites face additional reliability challenges. Replacement or repair of components is expensive and time-consuming due to difficulties accessing the site and dependency on good weather conditions. Thus, unscheduled down times as a result of component failure can lead to high operational and maintenance expenditures (O&M). For offshore wind turbines the O&M expenditures can reach 34 % of the levelised cost of energy (LCOE) [2]. A major contributor to the O&M expenditures is the gearbox with a failure rate of 0.1 - 0.15/year and average downtimes of 6 days per failure [3,4]. Early detection of gearbox faults is realized by fault prognosis methods based on sensor input from Supervisory Control and Data Analysis (SCADA) and Condition Monitoring Systems (CMS). Commercial fault prognosis systems analyse trends of health indicators extracted from sensor data, that correlate with the damage progression [5]. This purely data-driven approach has its strengths in detecting patterns indicating faulty behaviour from large, complex data sets without the need of modelling the system's behaviour. The drawbacks of data-driven methods often lie in the limited availability of historical failure data or expert knowledge for training, low generalizability across assets and lack of insight into of possible failure causes. A hybrid approach tries to circumvent some of these limitations by incorporating physics-based models in the fault prognosis process, see for example [6,7]. For the hybrid approach knowledge of the load history at critical locations in the gearbox (bearings, gear contacts) is essential as it allows the application of physical damage progression models such as fatigue [8], crack propagation [9] or frictional energy models [6]. In research local gearbox loads are generally calculated with computationally expensive simulations using aero-hydro-servo-elastic code in conjunction with multi-body simulation gearbox models, however this approach is

*Address all correspondence to this author.

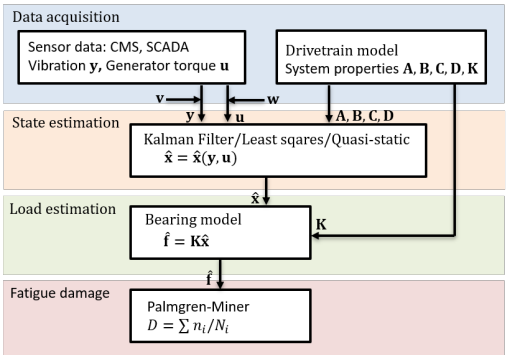

FIGURE 1: PROPOSED ONLINE FATIGUE MONITORING METHOD

not viable for real-time condition monitoring or fault prognosis. A more direct approach would be the reconstruction of gearbox loads from sensory data using inverse methods. Inverse methods have been developed to find solutions to the Inverse Problem, that is identifying excitation forces for a known dynamic state of a system [10]. A multitude of deterministic and probabilistic solutions are available, which have been reviewed by Sanchez et al. [11]. The most prominent applied methods in literature are Kalman filtering and least sqares estimators. Recent research has focused primarily on the identification of wind or wave loads on structural elements including aircraft [12], bridges [13], tall buildings [14–16] and wind turbine towers [17, 18]. A few studies also worked on machine elements with multi-body dynamics such as railway vehicles [19, 20], mining trucks [21] and diesel engines [22]. These results suggest, that this approach could also be applied to wind turbine drivetrains.

The detailed methodology is described in the following section. The proposed method is evaluated in a case study using a reference gearbox model and a reference load case. Estimated loads and loads from simulation measurements are compared using metrics in the time and frequency domain. Additionally, the relative error in fatigue damage based on estimated loads is analysed. Lastly, some concluding remarks are given.

METHODOLOGY

In this article a novel approach for the estimation of wind turbine gearbox loads with the purpose of online fatigue damage monitoring is presented (Fig. 1). The proposed method employs a Digital Twin framework and aims at continuous estimation of the dynamic states based on CMS vibration data and generator torque measurements from SCADA data. A case study is conducted to evaluate the proposed method using simulation measurements from high-fidelity drivetrain model, outlined in Sec. 2. The underlying linear physical model or Digital Twin for the load

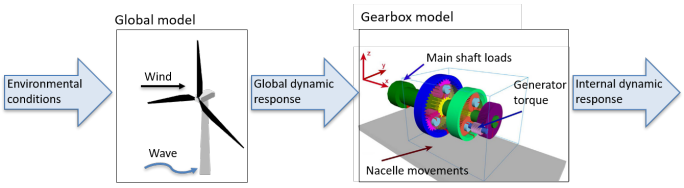

FIGURE 2: HIGH-FIDELITY PHYSICAL MODELS FOR VALIDATION OF THE PROPOSED METHOD

estimation method is developed in Sec. 3. Three state estimators with different levels of fidelity and requirements to sensory input are studied: Kalman Filter, Least Squares and a quasi-static approach (Sec. 4). With knowledge of the dynamic states local loads at gearbox bearings are easily determined and fatigue models, outlined in Sec. 5, are applied to track the accumulation of fatigue damage.

1 High-fidelity physical models

A reference gearbox based on the NREL offshore 5 MW baseline wind turbine and mounted on the floating OC3 Hywind spar structure is considered in this study [23, 24]. The reference gearbox was developed by Nejad et al. with reference to minimal weight and following offshore wind turbine design codes [25]. The gearbox comprises of two planetary and one parallel gear stage totalling to a gear ratio of 1:96.354. The main shaft support is a 4-point design with two main bearings to minimize non-torque loads entering the gearbox. A decoupled approach is employed, as shown in Fig. 2. The global response to a set of environmental conditions is determined with the global model, which is implemented in the aero-hydro-servo-elastic code SIMO-Riflex-AeroDyn. The internal dynamics are then simulated with a high-fidelity gearbox model implemented in the multi-body simulation environment SIMPACK. External loads (torque and non-torque) are applied on the main shaft, the nacelle movements are applied on the bed plate and the generator torque is applied on the HSS to control the generator speed.

2 Simulation measurements

Due to the lack of field measurements, simulation measurements from high-fidelity models are used in this study to evaluate the proposed load estimation method. A reference load case at rated wind speed of 12 m/s (load case EC4, spar in [26]) is simulated. The duration of the simulation is 3800 s, where the first 200 s are cut off to avoid simulation start-up effects. The simulation time step is 1 ms. From the simulation results the generator torque, shaft vibration and bearing loads are of interest. The generator torque and the shaft vibration are used to generate

synthetic SCADA and CM data as input for the load estimation method. Vibration signals are measured by virtual acceleration sensors mounted on the intermediate (IMS) and high-speed shaft (HSS) with a sampling frequency of 1 kHz. To capture yaw and pitch movements each shaft is equipped with two virtual sensors measuring axial and radial acceleration. White gaussian measurement noise $\mathbf{v} \sim \mathcal{N}(\mathbf{0}, \mathbf{R})$ is added to all acceleration measurements in postprocessing, where the covariance $\mathbf{R}$ is chosen, so that the signal-to-noise-ratio (SNR) is equal to 10 for all measurement signals. Additionally, the radial and axial loads at the IMS and HSS-bearings are extracted from simulation measurements for comparison with the estimated loads.

3 Linearized physical model

In the following section the high-fidelity drivetrain model is linearized and brought into state-space form, which is required for the state estimation algorithm discussed in Sec. 4. This study focuses on the bearing loads at the parallel gear stage. Hence, the system boundaries are set around the gear stage as depicted in Fig. 3. The system contains two moving rigid bodies, namely the shafts IMS and HSS with its rigidly connected gearwheels, and can be characterised as open-ended, meaning it is controlled by forces crossing the system boundaries. These are connection forces at the interfaces to the generator and the upwind planetary gear stage and are only partially known in this study. The forces on the generator side are fully defined with the generator torque, which is available through measurements. The loads on the IMS comprise of the known counteracting torque T_{IMS} and unknown disturbance forces f_{dis} from either internal dynamic excitations of upwind gear components, such as gear meshing of the planetary stages, or from external, non-torque, aerodynamic loads entering the gearbox. The model linearization is conducted with SIMPACKs built in linearization solvers, which compute the system matrices $\mathbf{A}, \mathbf{B}, \mathbf{C}, \mathbf{D}$ of the linear state-space representation. The general formulation of the linear state-space model is given by

$$\dot{\mathbf{x}} = \mathbf{A}\mathbf{x} + \mathbf{B}\mathbf{u} + \mathbf{w}, \tag{1}$$

$$\mathbf{y} = \mathbf{C}\mathbf{x} + \mathbf{D}\mathbf{u} + \mathbf{v}, \tag{2}$$

Eq. 1 is the state transition model, also referred to as the physical model in this paper, since it is derived from the equations of motion. Eq. 2 is the observation model and describes the relation of the system output to the states. In this case the state vector $\mathbf{x}$ is a stack of positions and velocities of the IMS and HSS relative to the gearbox housing. The input variable $\mathbf{u}$ is defined as the generator torque. The unknown disturbance forces $\mathbf{f_{dis}}$ are regarded as process noise with covariance $\mathbf{Q}$.The output variables $\mathbf{y}$ are measurements from virtual acceleration sensors on the IMS and HSS. The ouput is corrupted with measurement noise $\mathbf{v}$, which

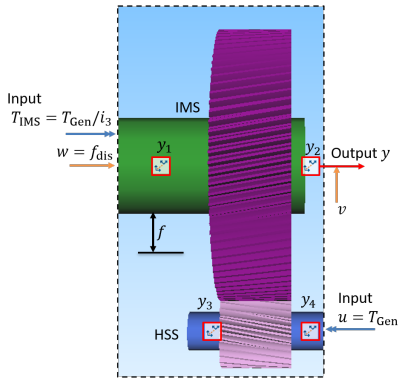

FIGURE 3: SYSTEM BOUNDARIES AND VARIABLE DEFINITION OF LINEARIZED MODEL

is modeled as white gaussian noise with covariance $\mathbf{R}$. In this case study measurement noise is added to the (exact) simulation measurements in postprocessing

$$\begin{aligned}
\mathbf{x} &:= [\tilde{\mathbf{x}}\ \dot{\tilde{\mathbf{x}}}]^{\mathrm{T}}, \\
\tilde{\mathbf{x}} &:= \tilde{\mathbf{x}}_{\mathrm{IMS,HSS}} - \tilde{\mathbf{x}}_{\mathrm{housing}} = [x\ y\ z\ \alpha\ \beta\ \gamma]^{\mathrm{T}} \\
\mathbf{u} &:= \mathrm{T}_{\mathrm{Gen}}, \\
\mathbf{y} &:= [\mathrm{y}_{\mathrm{rad}}\ \mathrm{y}_{\mathrm{ax}}]^{\mathrm{T}}_{1-4}, \\
\mathbf{w} &:= \mathbf{f}_{\mathrm{dis}} = [F_x\ F_y\ F_z\ M_x\ M_y\ M_z]^{\mathrm{T}} \sim \mathcal{N}(\mathbf{0}, \mathbf{Q}), \\
\mathbf{v} &\sim \mathcal{N}(\mathbf{0}, \mathbf{R}), \\
\mathbf{f} &:= [F_x\ F_y\ F_z\ ]^{\mathrm{T}}_{\mathrm{IMS/HSS-A,B,C}}.
\end{aligned} \tag{3}$$

In order to obtain the bearing loads $\mathbf{f}$ the general state-space model is augmented with an algebraic equation, which relates bearing loads to system states with the stiffness and damping matrix $\mathbf{K}$. Since the bearings are considered as spring-damper elements in the drivetrain model, this relationship is linear. The matrix $\mathbf{K}$ reflects the bearing stiffness and damping properties, as well as the transformation from body-fixed shaft coordinates to local bearing coordinates

$$\mathbf{f} = \mathbf{K}\mathbf{x}. \tag{4}$$

The continuous state-space model is discretized in time, where n indicates the time step

$$\mathbf{x_{n+1}} = \mathbf{A_d}\mathbf{x_n} + \mathbf{B_d}\mathbf{u_n} + \mathbf{w_n}, \tag{5}$$

$$\mathbf{y_n} = \mathbf{C}\mathbf{x_n} + \mathbf{D}\mathbf{u_n} + \mathbf{v_n}, \tag{6}$$

$$\mathbf{f_n} = \mathbf{K}\mathbf{x_n}. \tag{7}$$

The matrices $\mathbf{C}, \mathbf{D}, \mathbf{K}$ of the discrete model remain unchanged, as they only appear in algebraic equations, whereas $\mathbf{A_d}, \mathbf{B_d}$ are expressed as follows

$$\mathbf{A_d} = \exp(\mathbf{A}\Delta t), \tag{8}$$

$$\mathbf{B_d} = \mathbf{A}^{-1}(\mathbf{A_d} - \mathbf{I})\mathbf{B}. \tag{9}$$

4 Bearing load estimation

The load estimation is intended to be used for online monitoring applications and is thus conducted in the time domain for each time step n. Three different state estimators with different levels of fidelity and requirements to measurement inputs are studied, Kalman Filter, Least Squares and Quasi-static. In each case, the system states $\hat{\mathbf{x}}_\mathbf{n}$ are estimated first. Subsequently, the bearing loads are determined, as these are linear dependent on the system states

$$\hat{\mathbf{f}}_\mathbf{n} = \mathbf{K}\hat{\mathbf{x}}_\mathbf{n}. \tag{10}$$

4.1 Kalman Filter

The first load estimation method is based on Kalman filtering, which has been widely studied [13, 15–18, 21]. The Kalman Filter produces state estimates $\hat{\mathbf{x}}$ of a system, that is governed by stochastic, linear state equations as formulated in Eq. 5, 6 [27]. The optimal state estimates are determined by minimizing the estimate covariance, given by $\hat{\mathbf{P}} = \mathrm{cov}(\mathbf{x} - \hat{\mathbf{x}})$, which is a measure of the estimation accuracy. The algorithm involves a two-step process for each time step. In the prediction step the a priori state estimates $\hat{\mathbf{x}}_{\mathbf{n}|\mathbf{n-1}}$ are predicted with the physical model taking into account state estimates of the previous time step $\hat{\mathbf{x}}_{\mathbf{n-1}|\mathbf{n-1}}$ and known input variables $\mathbf{u_n} = \mathbf{T_{Gen}}$. The disturbance forces and moments $\mathbf{f_{dis}}$ on the system are not included in the prediction step, as they are regarded as process noise. The a priori estimated covariance $\hat{\mathbf{P}}_{\mathbf{n-1}|\mathbf{n-1}}$ is also predicted based on previous knowledge and the known process noise covariance Q

$$\hat{\mathbf{x}}_{\mathbf{n}|\mathbf{n-1}} = \mathbf{A_d}\hat{\mathbf{x}}_{\mathbf{n-1}|\mathbf{n-1}} + \mathbf{B_d}\mathbf{u}_{\mathbf{n-1}}, \tag{11}$$

$$\hat{\mathbf{P}}_{\mathbf{n}|\mathbf{n-1}} = \mathbf{A_d}\hat{\mathbf{x}}_{\mathbf{n-1}|\mathbf{n-1}}\mathbf{A_d^T} + \mathbf{Q}. \tag{12}$$

In the second step the a priori state estimates are updated with measurements $\mathbf{y_n}$ resulting in the a posteriori state estimates $\mathbf{x}_{\mathbf{n}|\mathbf{n}}$

$$\mathbf{M_n} = \hat{\mathbf{P}}_{\mathbf{n}|\mathbf{n-1}}\mathbf{C^T}(\mathbf{C}\hat{\mathbf{P}}_{\mathbf{n}|\mathbf{n-1}}\mathbf{C^T} + \mathbf{R})^{-1}, \tag{13}$$

$$\hat{\mathbf{x}}_{\mathbf{n}|\mathbf{n}} = \hat{\mathbf{x}}_{\mathbf{n}|\mathbf{n-1}} + \mathbf{M_n}(\mathbf{y_n} - \mathbf{C}\hat{\mathbf{x}}_{\mathbf{n}|\mathbf{n-1}} - \mathbf{Du_n}), \tag{14}$$

$$\hat{\mathbf{P}}_{\mathbf{n}|\mathbf{n}} = (\mathbf{I} - \mathbf{M_n}\mathbf{C})\hat{\mathbf{P}}_{\mathbf{n}|\mathbf{n-1}}. \tag{15}$$

The measurement update is weighted with the Kalman gain $\mathbf{M_n}$, which relates the confidence in state predictions of the physical model to the confidence in the measurement. With a high confidence in the physical model ($\hat{\mathbf{P}}_{\mathbf{n}|\mathbf{n-1}} \to \mathbf{0}$) the Kalman gain approaches zero, hence, the measurements update is given a low weight. On the other hand, with a high confidence in the measurements ($\mathbf{R} \to \mathbf{0}$) the Kalman gain approaches $\mathbf{C^{-1}}$. In this case the measurements have a higher significance compared to state predictions.

4.2 Quasi-static approach

The quasi-static (QS) method employs a low-fidelity approach, where the bearing loads are considered stationary, reactionary forces proportional to the drivetrain torque. This approach is used in a similar fashion for the calculation of gear contact forces in [8]. Contrary to the Kalman Filter, the QS state estimates are solely based on the physical model (Eq. 5) and do not take into account vibration measurements (Eq. 6). Additionally, the assumption is made, that the drivetrain is in quasi-static equilibrium and that internal dynamics are negligible. In the case quasi-static of equilibrium, where $\mathbf{x_{n+1}} - \mathbf{x_n} = \mathbf{0}$, the physical model (Eq. 5) reduces to

$$\mathbf{0} = (\mathbf{A_d} - \mathbf{I})\mathbf{x_n} + \mathbf{B_d}\mathbf{u_n} + \mathbf{w_n}. \tag{16}$$

Consequently, the state estimates can directly be determined from the input variable (generator torque) by disregarding the process noise

$$\hat{\mathbf{x}}_{\mathbf{stat,n}} = -(\mathbf{A_d} - \mathbf{I})^{-1}\mathbf{B_d}\mathbf{u_n}. \tag{17}$$

4.3 Least squares approach

A least squares approach to inverse state and load estimation is applied in [14, 19, 20]. This approach can be thought of as an asymptotic version of the Kalman Filter with high confidence in the measurements and low confidence in the physical model. In this case only the observation model (Eq. 6) of the state-space model is considered

$$\mathbf{y_n} = \mathbf{Cx_n} + \mathbf{Du_n} + \mathbf{v_n}. \tag{18}$$

The state estimates are found by minimizing the least squares error function

$$\hat{\mathbf{x}}_{\mathbf{LS,n}} = \arg\min_{\mathbf{x_n}}(\mathbf{y_n} - \mathbf{Cx_n} - \mathbf{Du_n})^\mathbf{T}(\mathbf{y_n} - \mathbf{Cx_n} - \mathbf{Du_n}). \tag{19}$$

The solution of the least-squares problem in closed form is given with the the Moore-Penrose pseudoinverse $\mathbf{C}^+$

$$\hat{\mathbf{x}}_{\mathbf{LS,n}} = \mathbf{C}^+(\mathbf{y_n} - \mathbf{Du_n}). \tag{20}$$

5 Fatigue damage

For evaluation of the proposed method the relative fatigue damage error is calculated, where $\hat{D}$ and D are the fatigue damage based on estimated and measured bearing loads respectively

$$e = \frac{\hat{D} - D}{\hat{D}}. \tag{21}$$

The Palmgren-Miner linear damage hypothesis is assumed for calculation of the fatigue damage, where n_i denote the experienced stress cycles, N_i the number of cycles until failure and i indicates the stress range

$$D = \sum_i \frac{n_i}{N_i}. \tag{22}$$

For calculation of N_i the nominal bearing life equation with the basic dynamic load rating C and the equivalent bearing load P is used

$$N_i = \left(\frac{C}{P}\right)^{\frac{10}{3}}. \tag{23}$$

P is a linear combination of the axial and radial load with the factors X and Y, which are bearing specific values taken from manufacturer's data

$$P = X \cdot F_{ax} + Y \cdot F_{rad}. \tag{24}$$

The stress cycles n_i are counted with the load distribution method according to IEC 61400-4 [28]. The LDD method is applicable for rotating machinery components under slowly varying loads, that experience cyclic loading due to entering and exiting the load zone each rotation. One stress cycle is counted for each rotation with a stress range equal to the current load.

DISCUSSION OF RESULTS

The inverse load estimation methods Kalman Filter (KF), Least Square (LS) and Quasi-Static (QS) presented in Sec. 4 are evaluated in a case study. The estimated radial loads at the IMS and HSS bearings are compared to simulation measurements obtained from the high-fidelity drivetrain model outlined in Sec. 2. First, the correlation of estimated and measured loads is analyzed in the time and frequency domain. Secondly, the error in calculated fatigue damage is discussed.

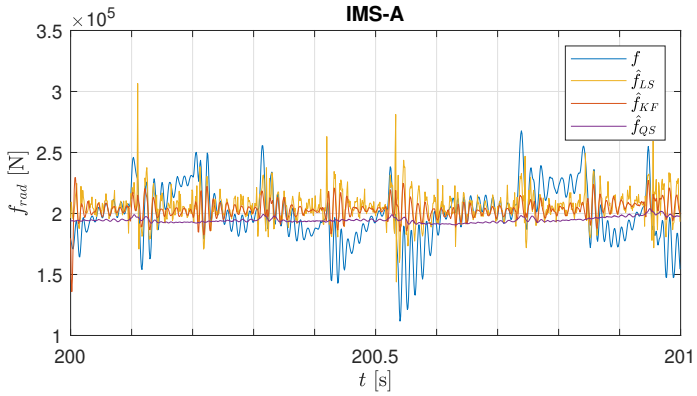

FIGURE 4: REPRESENTATIVE SECTION OF TIME SERIES OF MEASURED AND ESTIMATED LOADS AT IMS-A

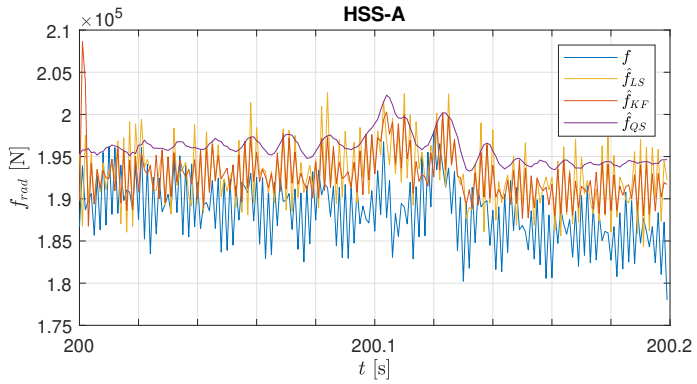

FIGURE 5: REPRESENTATIVE SECTION OF TIME SERIES OF MEASURED AND ESTIMATED LOADS AT HSS-A

6 Estimated loads

For a qualitative assessment a representative section of the time series of measured and estimated radial loads in the IMS-A and HSS-A bearings are shown in Fig. 4, 5. Notice the different time scales of the figures. The measured loads f are highly dynamic with components in both lower (< 10 Hz) and higher frequencies (> 100 Hz) and are offset by a non-zero mean value. The load estimates of the QS method $\hat{f}_{QS}$ are quasi-static with oscillations of small amplitudes and do not reflect the dynamics of measured loads. The mean value of measured loads is matched quite well by the QS method, although at the HSS-A a slight bias is observed. The LS method produces load estimates $\hat{f}_{LS}$ with high frequency oscillations of similar amplitudes to measured loads, however at the IMS-A there appear to be several outliers, which significantly overestimate measured loads. In the low-frequency range the LS method is not able to fully capture the internal gearbox dynamics. This is especially noticeable at the IMS-A, where the measured loads have a high-energy frequency component of about 5 Hz. The KF load estimates $\hat{f}_{KF}$

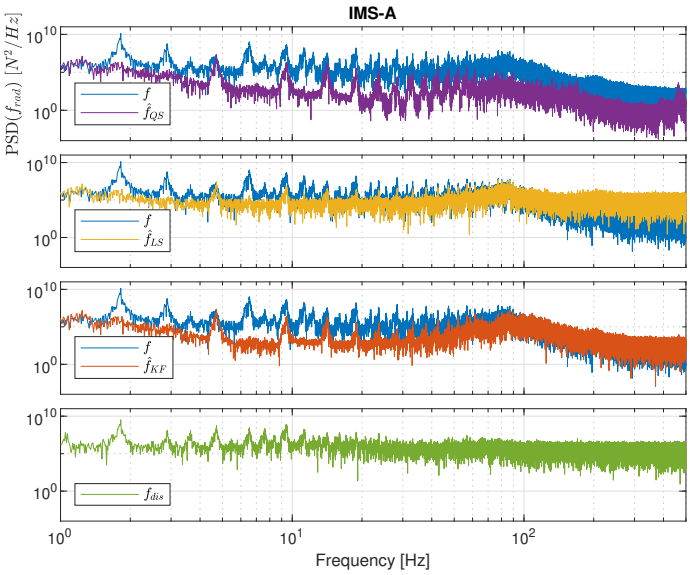

FIGURE 6: PSD OF MEASURED AND ESTIMATED RADIAL AT IMS-A LOADS FOR FULL TIME SERIES (3600 s).

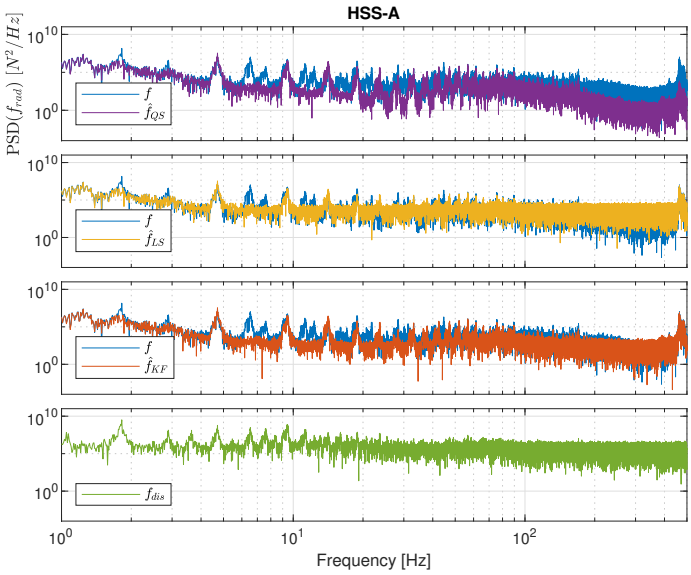

FIGURE 7: PSD OF MEASURED AND ESTIMATED RADIAL LOADS AT HSS-A FOR FULL TIME SERIES (3600 s).

are smoother and do not suffer from extreme outliers. Similar to the LS method high frequency oscillations are captured well, while some lower frequency components are not reflected.

For analysis of the behaviour in the frequency domain the power spectral densities (PSD) of measured and estimated bearing loads are calculated, as shown in Fig. 6, 7. The measured load spectrum shows several lower-frequency peaks ($<$ 10 Hz) and higher-frequency peaks at 80 Hz for IMS-A and at 464.2 Hz for HSS-A. The higher frequency peaks coincide with the gear meshing frequencies of the parallel and second planetary gear stage respectively. The lower frequency peaks are not fully identified as of now.

The QS method matches the measured load spectrum of HSS-A reasonably well with the exception of the high-frequency range with the gear meshing peak, which is underestimated significantly. In the low frequency range the peaks at 4.75 Hz, 9.47 Hz and 14.22 Hz are matched. These likely correspond to pure torsional oscillations of the HSS, which directly translate to oscillations in the generator torque. The dynamics of the IMS are not represented well with the QS method, as the QS load spectrum shows significantly lower energy in all frequencies.

In addition to the torsional oscillation peaks both the LS and KF method are able to match the gear meshing peaks. In the high-frequency range the LS method leads to a significant overestimation due to a high confidence in noisy measurements. The KF load estimates achieve a higher correlation by weighing the measurement update according to the measurement noise covariance R and thus filtering outliers. In the lower frequency range some peaks at 1.83 Hz, 2.91 Hz and 6.58 Hz, which are more pronounced at the IMS-A, are missed by both the LS and KF method.

The missed lower-frequency peaks likely relate to radial disturbance forces f_{dis} on the IMS, as the spectrum of measured disturbance forces suggests. The measured disturbance forces are extracted from the high-fidelity drive train simulations as connection forces of the second planetary gear stage to the IMS and show several low-frequency components of higher energy. The load estimation methods are unable to take these into account via state predictions, since the disturbance forces are assumed as white gaussian process noise in the underlying physical model. Furthermore, it is challenging to consider low-frequency disturbance force excitations via vibration measurements, because these cause relatively low acceleration responses with a low signal-to-noise-ratio.

For a quantitative assessment of the load correlation the Pearson correlation coefficient is calculated for the complete time series of 3600 s, as shown in Tab. 1. The correlation of IMS loads is quite poor, as the studied methods are unable to reproduce aforementioned low frequency load components. The KF is the best performing method, resulting in correlation values of 0.50 to 0.61. At the HSS the QS method is sufficient to estimate bearing loads with high correlation ($R > 0.8$), as internal dynamics have less significance here. The LS and KF method do not lead to significant improvements at the HSS.

TABLE 1: CORRELATION OF ESTIMATED LOADS

	QS	LS	KF
IMS-A	0.36	0.48	0.50
IMS-B	0.43	0.37	0.58
IMS-C	0.42	0.35	0.61
HSS-A	0.96	0.95	0.96
HSS-B	0.82	0.83	0.85
HSS-C	0.84	0.84	0.83

TABLE 2: FATIGUE DAMAGE ERROR

	QS [%]	LS [%]	KF [%]
IMS-A	11.8	11.6	12.3
IMS-B	5.7	0.8	3.8
IMS-C	-9.4	-13.6	-11.1
HSS-A	-5.2	-6.1	-5.9
HSS-B	10.7	8.3	8.5
HSS-C	15.2	11.2	11.4

7 Fatigue damage

Tab. 2 shows the relative fatigue damage error for the IMS and HSS bearings. The QS method results in low errors of 5 - 15 % across all bearings in the considered load case. The results of the higher fidelity methods LS and KF differ only marginally from those of the QS method despite considering internal dynamics and providing load estimates of higher correlation. The error can be slightly reduced at the bearings IMS-B and HSS-B,C, however at the bearings IMS-C and HSS-A a slightly higher error is calculated. These results suggest, that for the considered load case and drive train design the fatigue damage at the IMS and HSS bearings is mainly dependent on the drive train torque and effects of internal gearbox dynamics are negligible. This becomes more clear, when looking at the bearing stress cycles, which are not only a function of the load oscillations depicted in Fig. 4, but also of the rotational speed [8]. A rotating bearing experiences cyclic loading due to entering and exiting the load zone. This is reflected in the use of the stress cycle counting method LDD as opposed to the rainflow counting (RFC) method, which is commonly used for structural elements. The LDD method counts one stress cycle per revolution with a stress range equal to the current radial load. Thus, the quasi-static reactionary forces to the drive train torque cause major stress ranges and contribute significantly to the bearing fatigue, whereas the load variations from internal dynamics cause comparatively small stress ranges. In the studied load case at rated wind speed under normal operational conditions the QS method would be sufficient to monitor fatigue damage with high accuracy and computational speed. However, it is uncertain how the QS method would perform in load cases with greater internal dynamics, such as an emergency stop or gear faults. Further studies are planned to address this topic.

CONCLUSION

In this article a novel approach for the estimation of wind turbine gearbox loads with the purpose of online fatigue damage monitoring was presented. The proposed method employs a Digital Twin framework and aims at continuous estimation of the dynamic states based on CMS vibration data and generator torque measurements from SCADA data. The proposed method was evaluated in a load case at rated wind speed under normal operational conditions. With a quasi-static approach, which assumes proportionality to the drive train torque, the overall level of bearing loads were estimated with high accuracy, however the dynamic behaviour was not reflected well. The quasi-static method was sufficient to estimate fatigue damage with an error of 5-15 % across all bearings. The Kalman Filter approach produced the highest correlation of bearing loads ranging from 0.5-0.96 and was able to capture high-frequency dynamics accurately, but missed several low-frequency components. These are caused by disturbance forces on the IMS, which are not reflected in the underlying physical model and are not available through measurements. Despite considering internal dynamics, the KF method did not result in significant improvements with reference to fatigue damage. It appears, that in this load case the stress cycles caused by internal dynamics are insignificant relative to torque induced stress cycles. The Least-squares estimator performed worse than the Kalman Filter, as it is more sensitive to measurement noise. However, it has its advantages in computational speed, since it requires only one initial matrix inversion as opposed to the Kalman Filter with one matrix inversion for each time step. Further studies are planned to extend this work to different load cases or fault cases, assess the sensitivity to measurement noise and model uncertainties and quantify computational costs.

ACKNOWLEDGMENT

The authors wish to acknowledge financial support from the Research Council of Norway through InteDiag-WTCP project (Project number 309205).

REFERENCES

[1] Kumar, Y., Ringenberg, J., Depuru, S., Devabhaktuni, V. K., Lee, J., Nikolaidis, E., Andersen, B., and Afjeh, A., 2016. "Wind energy: Trends and enabling technologies". *Renewable and Sustainable Energy Reviews,* ***53***, pp. 209–224.

[2] Stehly, T., and Beiter, P., 2020. 2018 cost of wind energy review. Report, National Renewable Energy Laboratory.

[3] Faulstich, S., Hahn, B., and Tavner, P. J., 2011. "Wind turbine downtime and its importance for offshore deployment". *Wind Energy,* ***14***(3), pp. 327–337.

[4] Carroll, J., McDonald, A., and McMillan, D., 2016. "Failure rate, repair time and unscheduled o&m cost analysis of offshore wind turbines". *Wind Energy,* ***19***(6), pp. 1107–1119.

[5] Randall, R. B., 2010. *Vibration based condition monitoring: Industrial, Aerospace and Automotive Applications*. Wiley & Sons Ltd.

[6] Desai, A., Guo, Y., Sheng, S., Phillips, C., and Williams, L., 2020. "Prognosis of wind turbine gearbox bearing failures using scada and modeled data". *Annual conference of the prognostics and health management society*.

[7] Djeziri, M. A., Benmoussa, S., and Sanchez, R., 2018. "Hybrid method for remaining useful life prediction in wind turbine systems". *Renewable Energy,* ***116***, pp. 173–187.

[8] Nejad, A. R., Gao, Z., and Moan, T., 2014. "On long-term fatigue damage and reliability analysis of gears under wind loads in offshore wind turbine drivetrains". *International Journal of Fatigue,* ***61***, pp. 116–128.

[9] Dong, W., Nejad, A. R., Moan, T., and Gao, Z., 2020. "Structural reliability analysis of contact fatigue design of gears in wind turbine drivetrains". *Journal of Loss Prevention in the Process Industries,* ***65***.

[10] Gladwell, G. M., 2004. *Inverse Problems in Vibration*, Vol. 119 of *Solid mechanics and its applications*. Kluwer academic publishers.

[11] Sanchez, J., and Benaroya, H., 2014. "Review of force reconstruction techniques". *Journal of Sound and Vibration,* ***333***(14), pp. 2999–3018.

[12] Wang, L., and Liu, Y., 2020. "A novel method of distributed dynamic load identification for aircraft structure considering multi-source uncertainties". *Structural and Multidisciplinary Optimization,* ***61***(5), pp. 1929–1952.

[13] Petersen, Ø. W., Øiseth, O., and Lourens, E., 2019. "Full-scale identification of the wave forces exerted on a floating bridge using inverse methods and directional wave spectrum estimation". *Mechanical Systems and Signal Processing,* ***120***, pp. 708–726.

[14] Kazemi Amiri, A., and Bucher, C., 2017. "A procedure for in situ wind load reconstruction from structural response only based on field testing data". *Journal of Wind Engineering and Industrial Aerodynamics,* ***167***, pp. 75–86.

[15] Hwang, J.-S., Kareem, A., and Kim, H., 2011. "Wind load identification using wind tunnel test data by inverse analysis". *Journal of Wind Engineering and Industrial Aerodynamics,* ***99***(1), pp. 18–26.

[16] Zhi, L.-h., Fang, M.-x., and Li, Q. S., 2017. "Estimation of wind loads on a tall building by an inverse method". *Structural Control and Health Monitoring,* ***24***(4).

[17] Maes, K., Weijtjens, W., de Ridder, E. J., and Lombaert, G., 2018. "Inverse estimation of breaking wave loads on monopile wind turbines". *Ocean Engineering,* ***163***, pp. 544–554.

[18] Branlard, E., Giardina, D., and Brown, C. S. D., 2020. "Augmented kalman filter with a reduced mechanical model to estimate tower loads on a land-based wind turbine: a step towards digital-twin simulations". *Wind Energy Science,* ***5***(3), pp. 1155–1167.

[19] Zhu, T., Xiao, S., Yang, G., Ma, W., and Zhang, Z., 2013. "An inverse dynamics method for railway vehicle systems". *Transport,* ***29***(1), pp. 107–114.

[20] Uhl, T., 2006. "The inverse identification problem and its technical application". *Archive of Applied Mechanics,* ***77***(5), pp. 325–337.

[21] Siegrist, P. M., and McAree, P. R., 2006. "Tyre-force estimation by kalman inverse filtering: applications to off-highway mining trucks". *Vehicle System Dynamics,* ***44***(12), pp. 921–937.

[22] Leclère, Q., Pezerat, C., Laulagnet, B., and Polac, L., 2005. "Indirect measurement of main bearing loads in an operating diesel engine". *Journal of Sound and Vibration,* ***286***(1-2), pp. 341–361.

[23] Jonkman, J., Butterfield, S., Musial, W., and Scott, G., 2009. Definition of a 5-mw reference wind turbine for offshore system development. Report, National Renewable Energy Laboratory (NREL).

[24] Jonkman, J., 2010. Definition of the floating system for phase IV of OC3. Report, National Renewable Energy Laboratory (NREL).

[25] Nejad, A. R., Guo, Y., Gao, Z., and Moan, T., 2016. "Development of a 5 mw reference gearbox for offshore wind turbines". *Wind Energy,* ***19***(6), pp. 1089–1106.

[26] Nejad, A. R., Bachynski, E. E., Kvittem, M. I., Luan, C., Gao, Z., and Moan, T., 2015. "Stochastic dynamic load effect and fatigue damage analysis of drivetrains in land-based and tlp, spar and semi-submersible floating wind turbines". *Marine Structures,* ***42***, pp. 137–153.

[27] Welch, G.; Bishop, G., 1997. "An introduction to the kalman filter".

[28] IEC 61400-4, 2012. Wind turbines, part 4: standard for design and specification of gearboxes.